21st Australasian Fluid Mechanics Conference
Adelaide, Australia
10-13 December 2018

Changes in the Near-Surface Hydrodynamics of a Monochromatic Gravity Wave Field due to a Cylindrical-Shaped Intrusion in the Liquid Surface

A. A. Prata Jr.[1], S. Felder[2], F. Flocard[2], J. M. Santos[3] and R. Stuetz[1]

[1]UNSW Water Research Centre, School of Civil and Environmental Engineering
UNSW Sydney, NSW, 2052, Australia

[2]Water Research Laboratory, School of Civil and Environmental Engineering
UNSW Sydney, NSW, 2052, Australia

[3]Departamento de Engenharia Ambiental
Universidade Federal do Espírito Santo, Vitória, ES, 29.060-970, Brazil

Abstract

The near-surface hydrodynamics in the area enclosed by a cylindrical-shaped skirt (40 cm diameter; walls 4 mm thick; inserted 4 cm in the water at rest) exposed to monochromatic deep-water gravity waves was studied. The cylindrical intrusion was positioned fixed at the centreline of a 3 m wide wave flume and was exposed to trains of monochromatic deep-water gravity waves, with two combinations of frequency and wave height in the range of interest for environmental applications. An Acoustic Doppler Velocimeter (ADV) under the centre of the skirt was employed for the measurement of the 3D components of the water velocity. Compared against the background situation without the cylindrical intrusion, the presence of the skirt increased the magnitude of the turbulent velocity fluctuations and the rate of dissipation of turbulent kinetic energy, and interfered with the orbital wave-induced velocity.

Introduction

Enclosure devices are widely used for the sampling of atmospheric pollutants emitted from liquid surfaces, such as wastewater treatment plants, liquid waste storage tanks, reservoirs and wetlands (for instance, see [1,11,14]). However, there is a concern that the presence of the enclosure device can significantly interfere with the mass transfer conditions in the liquid and gas phases, leading to a biased assessment of the emissions [7,11]. Cylindrical-shaped skirts intruding into the water surface are a common feature of many enclosure devices, especially flux hoods (or flux chambers). Therefore, it is of great interest to understand how the presence of these intrusions in the liquid surface affects the near-surface hydrodynamics of the wave fields, which in turn is a critical factor controlling the inter-phase mass transfer.

In the liquid side, the rate of dissipation of turbulent kinetic energy (ε) has been identified as a potential key variable characterising this process [9,11,15]. Using velocity measurements from an Acoustic Doppler Velocimeter (ADV), Vachon et al. [11] calculated ε at 10 cm depth below the centre of the area enclosed by a sampling chamber (rectangular shape, with a skirt intruding 6 cm in the water) floating on lakes. In general, they found that the values of ε below the chamber were one order of magnitude larger than the corresponding ε outside the chamber, and attributed this to the "extra" turbulence generated by the movement of the chamber. Those authors also highlighted the need for a better understanding of the way intrusions in the water surface influence the turbulence below sampling chambers.

In this context, the present paper presents our initial findings on the near-surface hydrodynamics in the area enclosed by a cylindrical-shaped skirt exposed to monochromatic deep-water gravity waves, with focus on changes in the value of ε due to the intrusion in the liquid surface.

Methodology

Experimental Setup and Operation

The cylindrical-shaped skirt had a cylindrical body (diameter of 40 cm, total height 17.8 cm), with walls made of acrylic 4 mm thick, and was inserted 4 cm in the water at rest. These dimensions and insertion depth were chosen so as to represent a configuration commonly used for sampling hoods [1,4]. The skirt was positioned fixed at the centreline of a 3 m wide wave flume, with the centre of the circular footprint 3.16 m away from the wave paddle. The (undisturbed) water depth in the flume was kept constant at 0.85 m. An ADV (Vectrino+ VNO 1301, Nortek USA; acoustic frequency 10MHz) was mounted underneath the centre of the cylindrical skirt, with the transmitter pointing towards the water surface, using an adjustable metallic support that allowed the variation of the depth (h_{vel}) of the ADV sampling volume. The 3D components of the water velocity were measured by the ADV at a sampling frequency 200 Hz; additional settings of the ADV were: velocity range ± 0.30 m s^{-1}; transmit length of 1.8 mm; height of the sampling volume 2.5 mm; and power level "high". Two values of h_{vel}, 5 cm and 10 cm below the undisturbed water level, were tested. Figure 1 schematically illustrates the positioning of the ADV in relation to the cylindrical body of the surface intrusion.

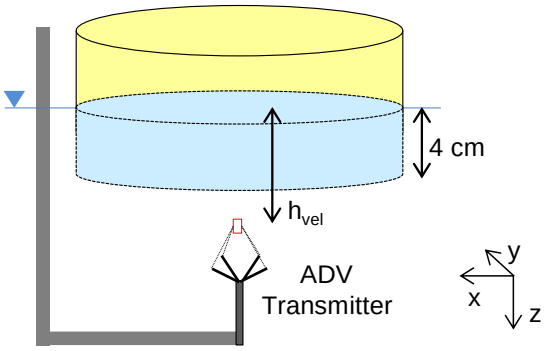

Figure 1. Schematic representation of the cylindrical body of the surface intrusion and the position of the ADV transmitter. The red rectangle represents the ADV sampling volume, at a depth h_{vel} below the level of the undisturbed water surface. The reference axes of the ADV measurements are also shown; the direction of wave propagation is from right to left (positive x).

Trains of monochromatic deep-water gravity waves were mechanically generated by a wave paddle, with two combinations of frequency (f) and wave height (H) in the range of interest for environmental applications [8], identified here as Conditions I and II. To characterise the wave field,

capacitance wave probes were applied to record the elevation of the water surface at frequency 100 Hz, at three transversal positions across the flume (aligned with the centre of the surface intrusion). Table 1 presents the nominal values of f and H, and the ranges of f_p (frequency of the peak of the wave spectra) and H_s (significant wave height) recorded by one of the wave probes (located 45.5 cm away from the centreline of the flume; the values recorded by the other two wave probes were similar) across the experimental runs, for each of the wave conditions. It is worth mentioning that Condition II presents steeper and more energetic waves than Condition I. In total, eight experimental runs were conducted: 2 wave conditions × 2 ADV sampling depths × 2 surface intrusion conditions (4 cm intrusion and background situation without the cylindrical intrusion). The number of valid waves in the wave trains for each run varied from 21 to 27 waves.

Variable	Condition I	Condition II
Nominal f (Hz)	1.57	1.65
Nominal H (mm)	38	53
Experimental f_p (Hz)	1.56 – 1.59	1.63 – 1.67
Experimental H_s (mm)	39 – 44	50 – 53

Table 1. Nominal values of f and H, and ranges of f_p and H_s recorded by one of the wave probes across the experimental runs, characterising the two wave conditions evaluated.

Processing of the ADV Data and Calculation of ε

The raw x,y,z-velocity time series measured by the ADV were preliminarily filtered using the software WinADV (version 2.0.0.28), selecting for minimum average correlation of 70% and signal-to-noise ratio (SNR) of 5, and applying the phase-space thresholding despiking technique proposed by Goring and Nikora [2], as modified by Wahl [12]. Since a few clear spikes were still present in the filtered series (changes in the correlation and SNR thresholds did not eliminate these spikes), a second filter was applied over the output from WinADV, discarding data for which the magnitude of the 3D velocity vector was larger than three standard deviations. The gaps in the time series of each velocity component were filled by linear interpolation. As an example, figure 2 shows the raw and processed z-velocity time series measured at h_{vel} = 10 cm, for Condition I, without the cylindrical intrusion.

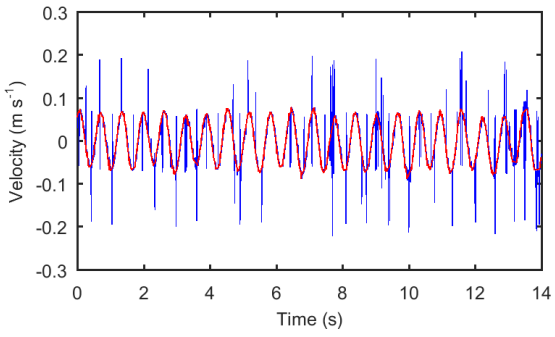

Figure 2. Raw (blue) and processed (red) z-velocity time series measured at h_{vel} = 10 cm, for Condition I, without the cylindrical intrusion.

According to Kolmogorov`s theory, for isotropic turbulence and high Reynolds numbers, the inertial subrange of the wavenumber power spectra of any of the components of the velocity can be described by equation 1:

$$P(k) = \alpha \varepsilon^{2/3} k^{-5/3} \quad (1)$$

Where k is the wavenumber (m^{-1}), and α is a dimensionless empirical constant (Kolmogorov`s constant).

Assuming Taylor`s [10] frozen turbulence hypothesis, the wavenumber power spectra can be converted into frequency power spectra, and equation 1 then becomes equivalent to equation 2, where $\overline{U}$ is the average advective velocity (m s^{-1}).

$$P(f) = \left(\frac{\overline{U}}{2\pi}\right)^{2/3} \alpha \varepsilon^{2/3} f^{-5/3} \quad (2)$$

Observing that the log–log plot of equation 2 is a straight line with slope -5/3, the interconversion between wavenumber and frequency power spectra allows the derivation of ε based on the time series resulting from the ADV measurements. To estimate ε from the ADV measurements, we used the frequency spectra of the processed z-velocity time series (which generally was the clearest signal). Following the practice adopted in other studies where wave motion was present [3,11], the power spectra were computed applying Welch`s [13] method (using the *pwelch* function built in Matlab`s Signal Processing Toolbox, with default settings). Having the frequency power spectra, ε was obtained by fitting a straight line with fixed slope -5/3 to the log–log plot of the power spectra over the inertial subrange (where equation 2 gives the variation of $P(f)$ with f), which results in equation 3:

$$\varepsilon = \left(\frac{2\pi}{\overline{U}}\right)\left\{\frac{exp\langle ln\left[P(f)f^{5/3}\right]\rangle}{\alpha}\right\}^{3/2} \quad (3)$$

Where the brackets $\langle\ \ \rangle$ indicate averaging over the inertial subrange.

The value $\alpha = 0.52$ was taken, following [11]. For situations where the wave orbital motion is the main responsible for the advection of the turbulent eddies, Lumley and Terray [6] recommend the use of the wave orbital velocity as the value of $\overline{U}$. In the present case, the wave orbital velocity was estimated as the time-average of the magnitude of the 3D velocity vector (after applying, to each of the velocity components, the filtering and gap-filling procedure previously discussed).

Results and Discussion

The processed z-velocity time series for the background situation (no intrusion) and for 4 cm intrusion are compared in figure 3, for wave Condition I and the two ADV sampling depths. For both depths, in the absence of the cylindrical intrusion, the variation of the z-velocity follows a distinctive pattern, consistent with the orbital motion of the waves. By contrast, the presence of the surface intrusion greatly affects the wave-coherent pattern of the z-velocity in the area enclosed by the cylindrical skirt. The same qualitative behaviour was observed for Condition II. Also, the amplitude of the z-velocity oscillations becomes smaller, whereas the small-scale, turbulent fluctuations of the velocity appear to become more intense with the presence of the surface intrusion. This last point is confirmed by the changes in the value of u, the standard deviation of the velocity magnitude (that is, the root-mean-square of the turbulent velocity fluctuations) shown in table 2.

h_{vel} (cm)	Intrusion	Condition I	Condition II
10	No	0.012	0.026
10	Yes	0.045	0.075
5	No	0.017	0.022
5	Yes	0.049	0.082

Table 2. Standard deviation of the magnitude of the 3D velocity vector (after applying, to each of the velocity components, the filtering and gap-filling procedure), in m s^{-1}.

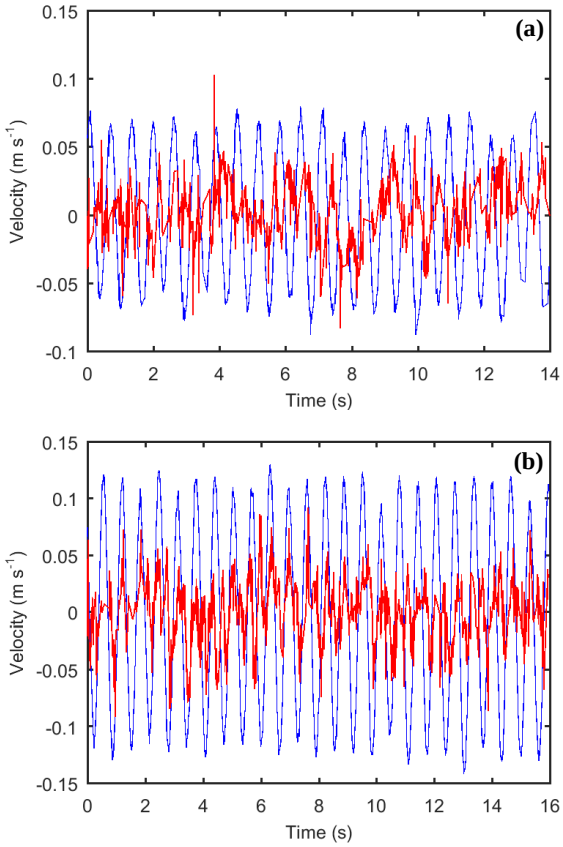

Figure 3. Processed z-velocity time series for the background situation (blue) and for 4 cm intrusion (red), for wave Condition I and ADV sampling depths h_{vel} = 10 cm (a) and h_{vel} = 5 cm (b).

It can be noticed in table 2 that the increase in u is larger for Condition II, which is a more energetic wave condition. It is also important to mention that the values of $(u/\overline{U})^3$ ranged from 0.004 to 0.267 (0.091 on average), attending the criteria $(u/\overline{U})^3 < 1$ recommended by Kitaigorodskii et al. [5] for the validity of Taylor`s hypothesis of frozen turbulence, which is one of the conditions for the calculation of ε by means of equation 3.

Figure 4 shows the frequency power spectra of the z-component of the velocity for the background case (without the surface intrusion) and for the case with 4 cm intrusion, for ADV sampling depth h_{vel} = 10 cm and for both wave conditions. The features of these power spectra reflect the behaviour of the z-velocity discussed in the previous paragraphs. For instance, a clear and highly energetic peak is observed around the nominal frequency of the waves, for the background cases (blue lines), whilst this peak is much less energetic for the cases with the surface intrusion (red lines). On the other hand, the energy spectral density at higher frequencies is considerably higher for the cases with the cylindrical intrusion, which is explained by the more intense turbulent fluctuations observed in the velocity measurements.

Table 3 presents the values of ε calculated from the power spectra shown in figure 4. Compared against the respective cases for Condition I, ε was invariably higher for Condition II, in which the waves were more energetic and the turbulence more intense. The value of ε at 10 cm depth for the background case and Condition I is within the range measured by Vachon et al. [11] 10 cm underneath the free surface of lakes, whereas the background ε calculated for Condition II is slightly above the upper limit of their range. This is possibly due to the fact that the waves of Condition II are likely more energetic than the waves in the lakes studied by [11], who report conditions of "low turbulence". In the presence of the cylindrical skirt, our results indicate a considerable increase in ε, of approximately one order of magnitude. The size of such increase is similar to the trend identified by [11] comparing ε inside and outside the area enclosed by a rectangular sampling chamber floating on lakes. Nonetheless, it is worth noting that the explanation given by [11] (that the increase in ε is due to turbulence generated by the movement of the chamber) is not applicable in our case, since the cylindrical skirt was kept fixed and unmoving. Thus, for the wave conditions and the geometry of the cylindrical intrusion evaluated herein, it can be hypothesised that the interaction of the wave motion with the wall of the intrusion was responsible for the observed changes in u and ε underneath the centre of the area enclosed by the skirt.

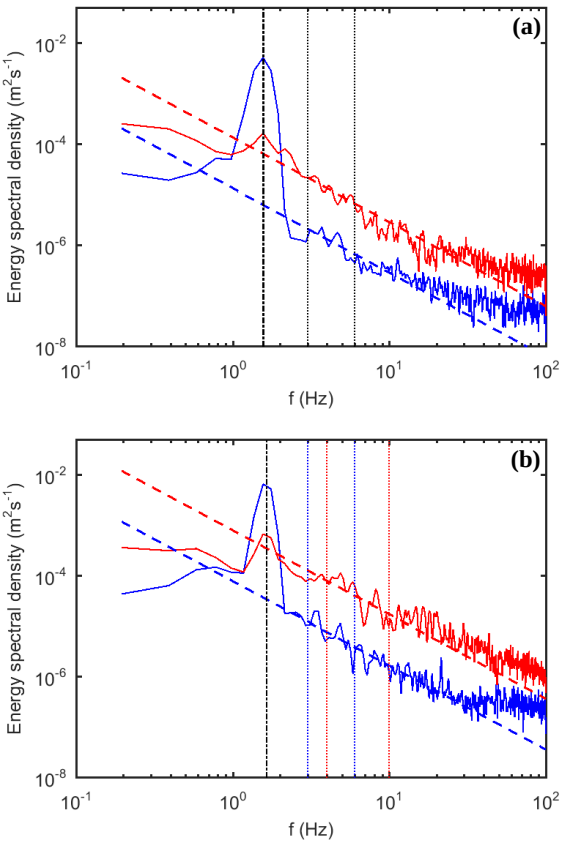

Figure 4. Frequency power spectra of the z-component of the velocity for the background situation (blue) and for 4 cm intrusion (red), for ADV sampling depth h_{vel} = 10 cm and for wave Condition I (a) and Condition II (b). The solid lines are the power spectra; the dashed lines represent the fit given by equation (2), with ε calculated by equation 3; the black vertical dash-dotted line indicates the nominal frequency of the waves; and the vertical dotted lines mark the limits of the inertial subrange considered for the calculation of ε. In (b), the limits of the inertial subrange were different for the background and 4 cm intrusion cases, and are identified by the dotted lines with respective colours (blue = background; red = 4 cm intrusion).

h_{vel} (cm)	Intrusion	Condition I	Condition II
10	No	1.27E-5	1.44E-4
10	Yes	3.29E-4	3.28E-3
5	No	1.47E-5	4.04E-5
5	Yes	5.08E-4	1.31E-3

Table 3. Rate of dissipation of turbulent kinetic energy (ε), in $m^2 s^{-3}$.

Conclusions

The near-surface hydrodynamics underneath the centre of the area enclosed by a cylindrical-shaped skirt exposed to monochromatic deep-water gravity waves was assessed by ADV velocity measurements at two distinct depths. Compared against the background situation without the cylindrical intrusion, the presence of the skirt: (i) affected the orbital wave-induced velocity; (ii) increased the magnitude of the turbulent velocity fluctuations; and (iii) increased the rate of dissipation of turbulent kinetic energy by one order of magnitude. Such changes in the hydrodynamics can be expected to have considerable implications for the use of enclosure sampling devices.

Acknowledgments

A. A. Prata Jr. acknowledges the institutional support of Coordenação de Aperfeiçoamento de Pessoal de Nível Superior (CAPES), Brazil.

References

[1] Eklund, B. Practical guidance for flux chamber measurements of fugitive volatile organic emission rates, *Journal of the Air & Waste Management Association*, **4**2, 1992, 1583–1591.

[2] Goring, D.G. & Nikora, V.I., Despiking Acoustic Doppler Velocimeter Data, *Journal of Hydraulic Engineering*, **128**, 200, 117–126.

[3] Huang, C.J., Ma, H., Guo, J., Dai, D. & Qiao, F., Calculation of turbulent dissipation rate with acoustic Doppler velocimeter, *Limnology and Oceanography: Methods*, **16**, 2018, 265–272.

[4] Kienbusch, M. *Measurement of gaseous emission rates from land surfaces using an emission isolation flux chamber – User`s Guide*. EPA 600/8-86-008 (NTIS PB86-223161), US EPA, Environmental Monitoring Systems Laboratory, Las Vegas, 1986.

[5] Kitaigorodskii, S.A., Donelan, M.A., Lumley, J.L. & Terray, E.A., Wave-Turbulence Interactions in the Upper Ocean. Part II. Statistical Characteristics of Wave and Turbulent Components of the Random Velocity Field in the Marine Surface Layer, *J. Phys. Oceanogr.*, **13**, 1983, 1988–1999.

[6] Lumley, J.L. & Terray, E.A., Kinematics of Turbulence Convected by a Random Wave Field, *J. Phys. Oceanogr.*, **13**, 1983, 2000–2007.

[7] Prata, A.A., Lucernoni, F., Santos, J.M., Capelli, L., Sironi, S., Le-Minh, N. & Stuetz, R.M., Mass transfer inside a flux hood for the sampling of gaseous emissions from liquid surfaces – Experimental assessment and emission rate rescaling, *Atmospheric Environment*, **179**, 2018, 227–238.

[8] Prata Jr., A.A., Santos, J.M., Timchenko, V., Reis, N.C. & Stuetz, R.M., Wind friction parametrisation used in emission models for wastewater treatment plants: A critical review, *Water Research*, **124**, 2017, 49–66.

[9] Prata Jr., A.A., Santos, J.M., Timchenko, V. & Stuetz, R.M., A critical review on liquid-gas mass transfer models for estimating gaseous emissions from passive liquid surfaces in wastewater treatment plants, *Water Research*, **130**, 2018, 388–406.

[10] Taylor, G.I., Statistical Theory of Turbulence. Proceedings of the Royal Society of London A: Mathematical, Physical and Engineering Sciences, **151**, 1935, 421–444.

[11] Vachon, D., Prairie, Y.T. & Cole, J.J., The relationship between near-surface turbulence and gas transfer velocity in freshwater systems and its implications for floating chamber measurements of gas exchange, *Limnology and oceanography*, **55**, 2010, 1723–1732.

[12] Wahl, T. L., Discussion of "Despiking Acoustic Doppler Velocimeter Data" by Derek G. Goring and Vladimir I. Nikora, *Journal of Hydraulic Engineering*, 129, 2003, 484–487.

[13] Welch, P., The use of fast Fourier transform for the estimation of power spectra: A method based on time averaging over short, modified periodograms, *IEEE Transactions on Audio and Electroacoustics*, **15**, 1967, 70–73.

[14] Xiao, S., Yang, H., Liu, D., Zhang, C., Lei, D., Wang, Y., Peng, F., Li, Y., Wang, C., Li, X., Wu, G. & Liu, L., Gas transfer velocities of methane and carbon dioxide in a subtropical shallow pond, *Tellus B*, **66**, 2014, 23795.

[15] Zappa, C.J., McGillis, W.R., Raymond, P.A., Edson, J.B., Hintsa, E.J., Zemmelink, H.J., Dacey, J.W. & Ho, D.T., Environmental turbulent mixing controls on air-water gas exchange in marine and aquatic systems, *Geophysical Research Letters*, **34**, 2007.